# Supplementary Information: A machine learning model that outperforms conventional global subseasonal forecast models

Lei Chen[1†], Xiaohui Zhong[1,2†], Jie Wu[3†], Deliang Chen[4], Shang-Ping Xie[5], Qingchen Chao[3], Chensen Lin[2], Zixin Hu[2], Bo Lu[3*], Hao Li[1,2*] and Yuan Qi[2,1*]

[1]Shanghai Academy of Artificial Intelligence for Science, Shanghai, 200232, China.
[2]Artificial Intelligence Innovation and Incubation Institute, Fudan University, Shanghai, 200433, China.
[3]China Meteorological Administration Key Laboratory for Climate Prediction Studies, National Climate Center, Beijing, 100081, China.
[4]University of Gothenburg, Sweden.
[5]Scripps Institution of Oceanography, University of California San Diego, USA.

*Corresponding author(s). E-mail(s): bolu@cma.gov.cn; lihao_lh@fudan.edu.cn; qiyuan@fudan.edu.cn;
Contributing authors: cltpys@163.com; x7zhong@gmail.com; wujie@cma.gov.com; deliang@gvc.gu.se; sxie@ucsd.edu; chaoqc@cma.gov.cn; linchensen@fudan.edu.cn; huzixin@fudan.edu.cn;
†These authors contributed equally to this work.

## Contents of this file

# Supplementary Notes

## 1 Deterministic forecast metrics comparison

Supplementary Figure 1 presents a comparison of the globally-averaged and latitude-weighted root mean square error (RMSE) of the ensemble mean between ECMWF S2S real-time forecasts and FuXi-S2S forecasts for total precipitation (TP), 2-meter temperature (T2M), geopotential at 500 hPa (Z500), and outgoing longwave radiation (OLR). The analysis is derived from the averaged RMSE computed using testing data from the year 2022. FuXi-S2S demonstrates superior forecast performance for all four variables across all forecast lead times compared to ECMWF S2S, consistently achieving lower RMSE) values than ECMWF S2S.

Supplementary Figure 3 presents a comparison of latitude-weighted TCC between FuXi-S2S and ECMWF S2S. It examines TP, T2M, Z500, and OLR across four geographical regions: in the extra-tropics (90°S - 30°S and 30°N - 90°N), in the tropics (30°S - 30°N), over land, and over the ocean. Within the extra-tropical regions, FuXi-S2S consistently exhibits superior performance compared to ECMWF S2S for all four variables. In tropical regions, FuXi-S2S outperforms ECMWF S2S for TP and OLR, while achieving comparable accuracy in T2M and Z500. Over land areas, FuXi-S2S demonstrates consistently higher TCC values for TP, Z500, and OLR.

## 2 Extreme Meiyu in 2020

The major rainy season of the East Asian summer monsoon, called Meiyu in China [1], typically starts in early June and ends in mid-July. This brings abundant rainfall which accounts for the majority of the annual precipitation in China, Japan, and South Korea [2, 3]. In the summer of 2020, the Yangtze-Huaihe River valley (YHRV) experienced an exceptionally intense Meiyu rainy season characterized by an earlier onset and a delayed retreat. This season lasted for 62 days, making it one of the longest events since 1961, equalling the duration of the 2015 event [4]. The accumulated precipitation during the 2020 Meiyu season broke the historical record since 1961 and resulted in the most severe flooding in the YHRV in recent decades. By mid-July, the flooding had led to more than 140 fatalities or missing persons and economic losses of USD 11.75 billion.

Figure 7 presents the comparison of the standardized TP anomaly among the observations sourced from Global Precipitation Climatology Project (GPCP), ECMWF S2S, and FuXi-S2S, averaged across YHRV bounded by 105 to 125°E in longitude and 25 to 35°N in latitude. The GPCP are temporally averaged over a two-week period from June 30th to July 13th, 2020, which corresponds to a low skill and cold-front rainy period as revealed by by Liu et al. [5]. FuXi-S2S forecasts and ECMWF S2S reforecasts were initialized on different dates. Notably, the ECMWF S2S model predicts negative TP anomalies for forecasts initialized on both June 2nd and June 6th. However, while

the ECMWF S2S model starts to predict positive TP anomalies from June 9th onwards, the model consistently underestimates rainfall intensity. In contrast, the FuXi-S2S model predicts positive anomalies for forecasts initialized as early as June 2nd, offering a lead time of 4 weeks prior to the occurrence of the event. Furthermore, the spatial distributions of the standardized TP anomaly reveals that TP patterns predicted by FuXi-S2S closely aligns with the observations, which is critical for flood preparedness. In summary, FuXi-S2S demonstrates superior performance in predicting the intensity of extreme rainfall events with longer lead time compared to ECMWF S2S.

# 3 Comparisons against ECMWF S2S real-time forecasts

This study also evaluates the performance of FuXi-S2S by analyzing testing data from 2022 and compare against the 51-member ECMWF S2S real-time forecasts from model cycle C47r3. The evaluation included deterministic metrics of the ensemble mean, ensemble metrics, and Madden–Julian Oscillation (MJO) forecasts.

Supplementary Figure 8 presents a comparison of the globally-averaged and latitude-weighted TCC, RMSE, RPSS, and BSS of the ensemble mean between the ECMWF S2S real-time forecasts and FuXi-S2S forecasts for TP in 2022. Across all forecast lead times, FuXi-S2S demonstrates superior forecast performance in all metrics across compared to the ECMWF S2S real-time forecasts.

Supplementary Figure 9 presents the bivariate correlation (COR) skills of Real-time Multivariate MJO (RMM) index for the ensemble mean of ECMWF S2S real-time forecasts and FuXi-S2S forecasts, averaged over the testing data from 2022. When applying a COR threshold of 0.5 to determine skillful MJO forecast, FuXi-S2S extends the skilful forecast lead time from 30 days to 41 days, surpassing the performance of ECMWF S2S real-time forecasts.

# 4 Effectiveness of flow-dependent perturbations

This section discusses the effect of incorporating the flow-dependent perturbations into the model's hidden features to enhance performance in subseasonal forecasts. We conducted experiments using FuXi-S2S models which exclusively employ Perlin noise in the initial conditions or combine Perlin noise in the initial conditions with fixed perturbations added into the hidden features, to generate 42-day forecasts. Subsequently we evaluate their performance in comparison with the original FuXi-S2S model.

Supplementary Figure 10 presents a comparison of the globally-averaged and latitude-weighted TCC for TP. This analysis encompasses all testing data from the period spanning from 2017 to 2021. The FuXi-S2S model, which incorporates flow-dependent perturbations into its hidden features, consistently exhibits considerably improved forecast performance in comparison to

the FuXi-S2S model that incorporates fixed Gaussian noise into the hidden features, across all forecast lead times. Furthermore, the introduction of flow-dependent perturbations has extended the FuXi-S2S model's skillful MJO prediction from 22 days to 36 days.

# Supplementary Figures

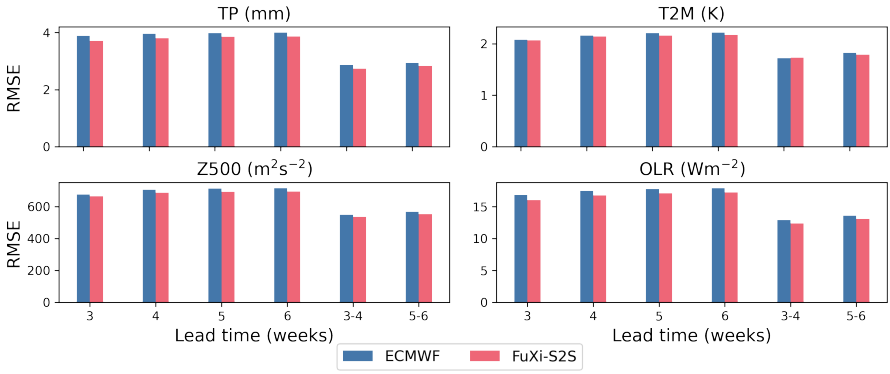


**Supplementary Figure 1**: Comparison of the globally-averaged and latitude-weighted RMSE of the ensemble mean between ECMWF S2S reforecasts (in blue) and FuXi-S2S forecasts (in red) for TP, T2M, Z500, and OLR, using all testing data between 2017 and 2021. It is important to note that TP here refers to 24-hour accumulated precipitation.

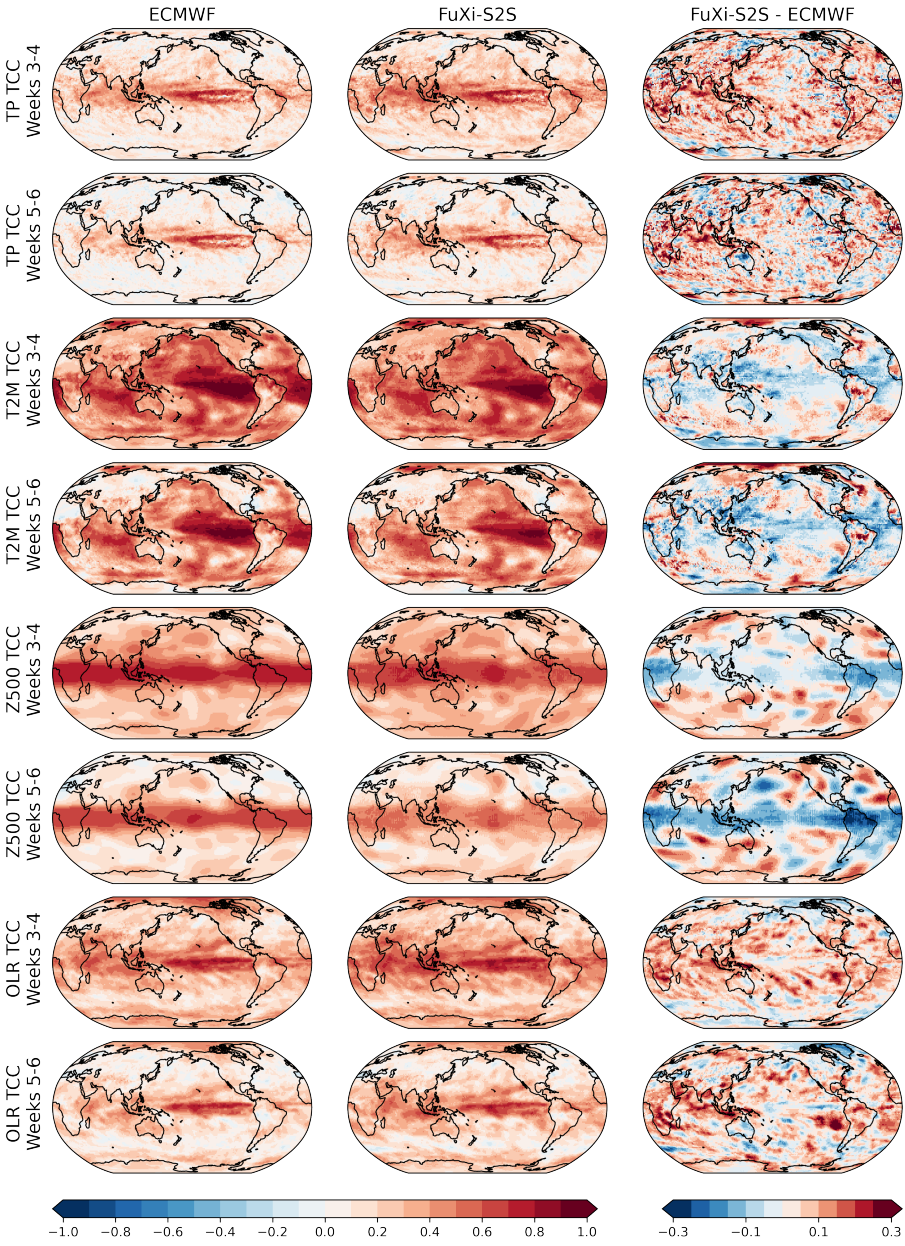


**Supplementary Figure 2**: Spatial map of average TCC without latitude weighting of ECMWF S2S (first column) and FuXi-S2S (second column), and the differences in TCC between FuXi-S2S and ECMWF S2S (third column) for TP (first and second rows), T2M (third and fourth rows), Z500 (fifth and sixth rows), and OLR (seventh and eighth rows) at forecast lead times of weeks 3-4 (first, third, fifth, and seventh rows), weeks 5-6 (second, fourth, sixth, and eighth rows), using all testing data between 2017 and 2021.

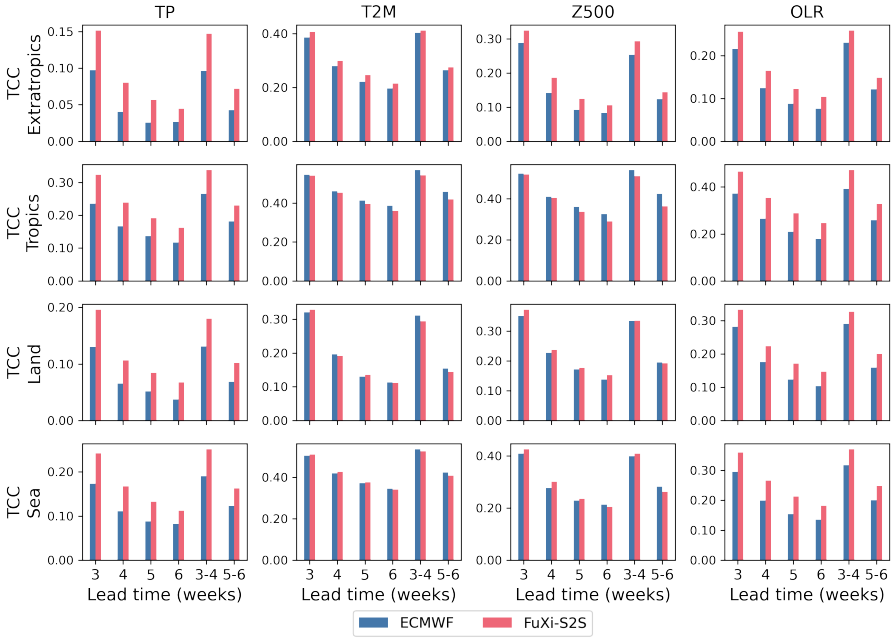


**Supplementary Figure 3**: Comparison of the latitude-weighted TCC of the ensemble mean of ECMWF S2S (in blue) forecasts and FuXi-S2S forecasts (in red) for TP (first column), T2M (second column), Z500 (third column), and OLR (fourth column) averaged over extra-tropics (90°S - 30°S and 30°N - 90°N, first row), tropics (30°S - 30°N, second row), land (third row), and sea (fourth row), using all testing data between 2017 and 2021

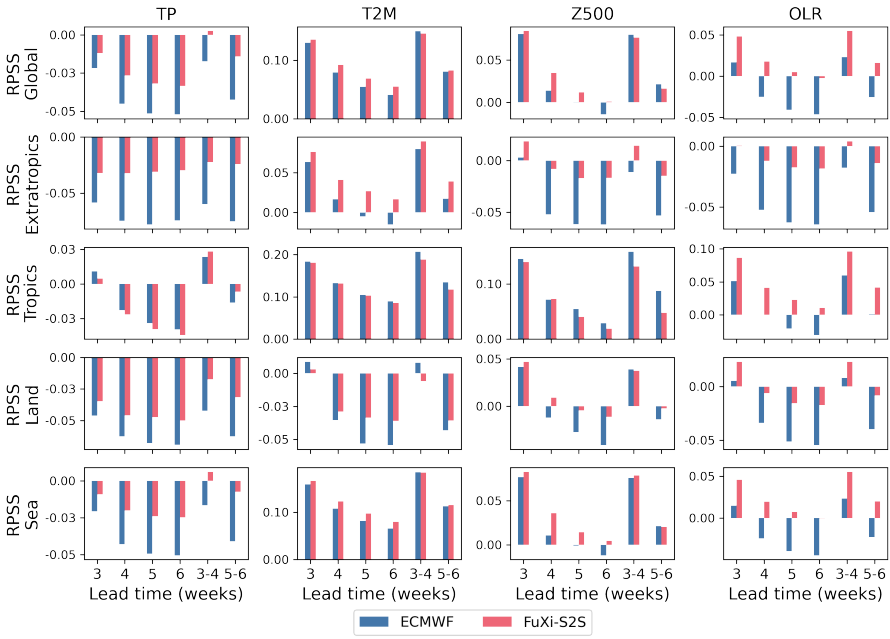


**Supplementary Figure 4**: Comparison of the latitude-weighted RPSS of the ensemble mean of ECMWF S2S (in blue) forecasts and FuXi-S2S forecasts (in red) for TP (first column), T2M (second column), Z500 (third column), and OLR (fourth column) averaged over extra-tropics (90°S - 30°S and 30°N - 90°N, first row), tropics (30°S - 30°N, second row), land (third row), and sea (fourth row), using all testing data between 2017 and 2021.

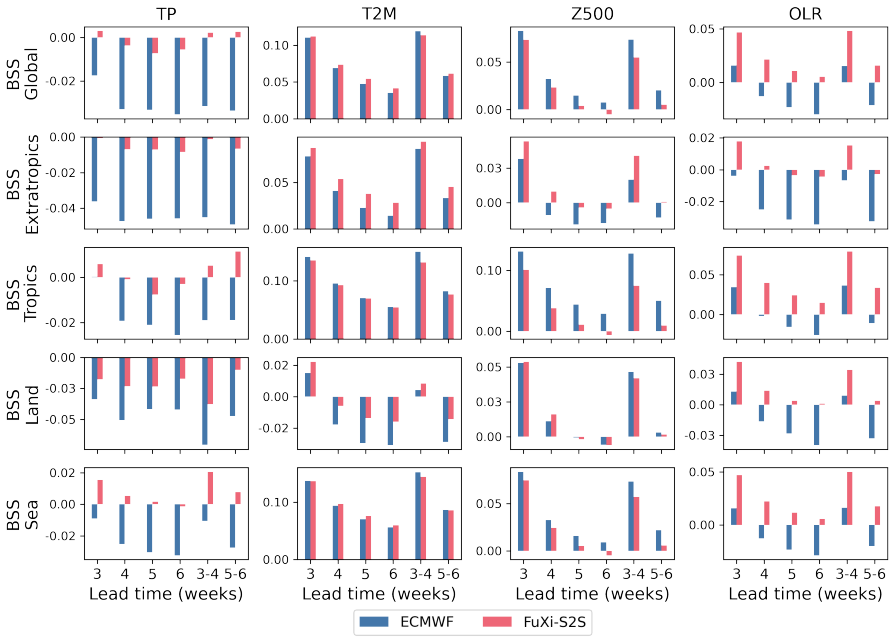


**Supplementary Figure 5**: Comparison of the latitude-weighted BSS of the ensemble mean of ECMWF S2S (in blue) forecasts and FuXi-S2S forecasts (in red) for TP (first column), T2M (second column), Z500 (third column), and OLR (fourth column) averaged over extra-tropics (90°S - 30°S and 30°N - 90°N, first row), tropics (30°S - 30°N, second row), land (third row), and sea (fourth row), using all testing data between 2017 and 2021.

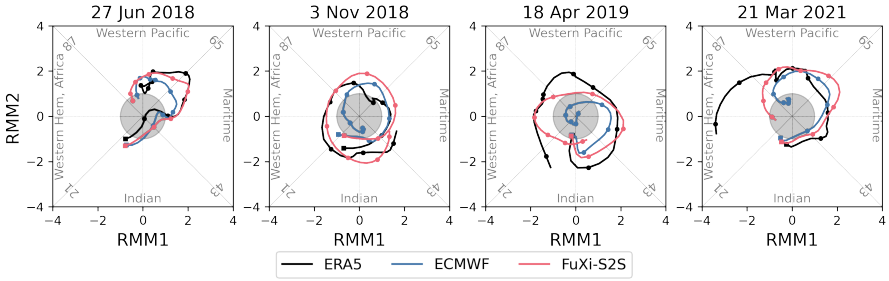


**Supplementary Figure 6**: Comparison of the RMM composite phase–space diagram for the observed MJO derived from the combination of CBO and ERA5 reanalysis data (in black) and the ensemble mean of ECMWF S2S reforecasts (in blue), and FuXi-S2S forecasts (in red). RMM1 and RMM2 are the x axis and y axis, respectively. The numbers within each octant (from 1 to 8) are the defined MJO phase, and the words on each side of the diagram describe the approximate location of MJO associated convection along the equator. Squares represent forecasts on day 1 and closed circles represent every 5 days from the forecast initialization time (open squares). The panels are for different initialization date: 27 June 2018, 3 November 2018, 18 April 2019, and 21 March 2021.

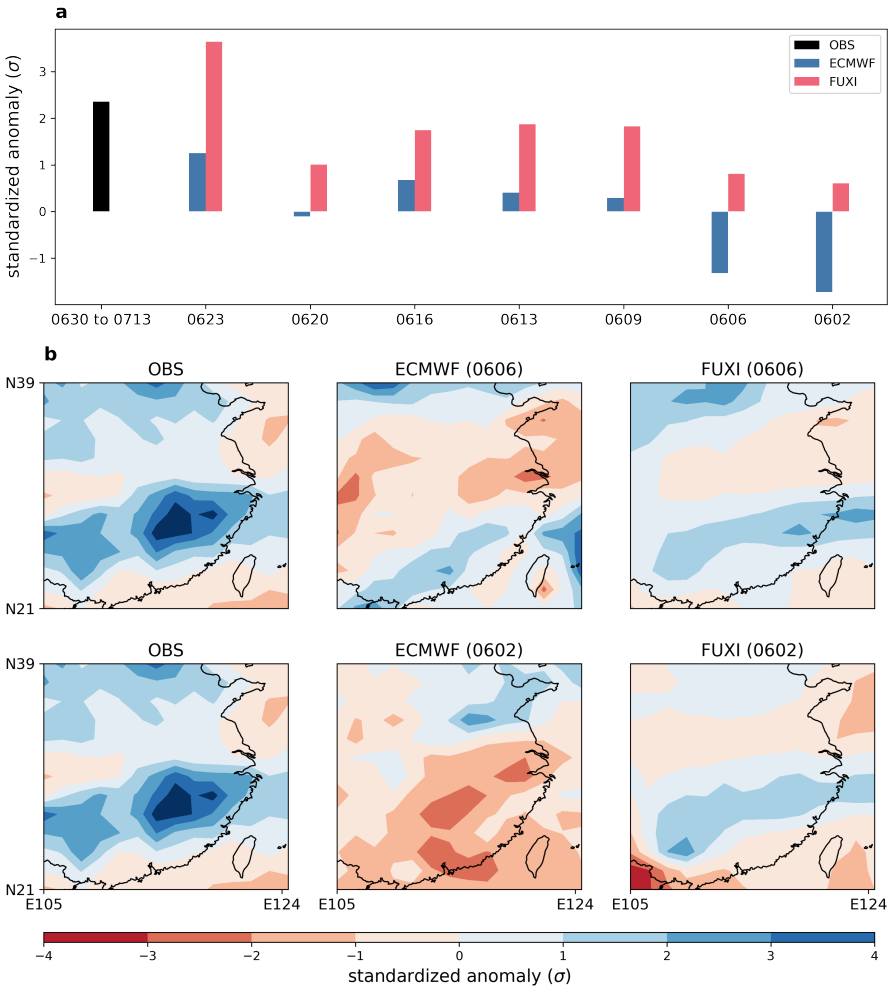


**Supplementary Figure 7**: Comparison of the spatially and temporally averaged standardised TP anomaly (a) for the 2 weeks from June 30th to July 13th, 2020 for GPCP observation (in black) and the predictions from ECMWF S2S reforecasts (in blue) and FuXi-S2S forecasts (in red), with initialization dates: June 23rd (0623), June 20th (0620), June 16th (0616), June 13th (0613), June 9th (0609), June 6th (0606), and June 2nd (0602). Comparison of the temporally averaged standardised TP anomaly maps (b) for GPCP observation (first column) and predictions from ECMWF S2S (second column) and FuXi-S2S (third column), with initialization dates on June 6th (0606, first row), and June 2nd (0602, second row).

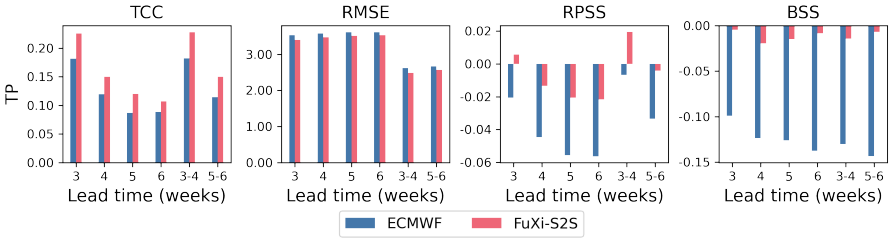


**Supplementary Figure 8**: Comparison of the globally-averaged latitude-weighted TCC (first column), RMSE (second column), RPSS (third column), and BSS (fourth column) of the ensemble mean between ECMWF S2S real-time forecasts (in blue) and FuXi-S2S forecasts (in red) for TP, using testing data from 2022. It is important to note that TP here refers to 24-hour accumulated precipitation.

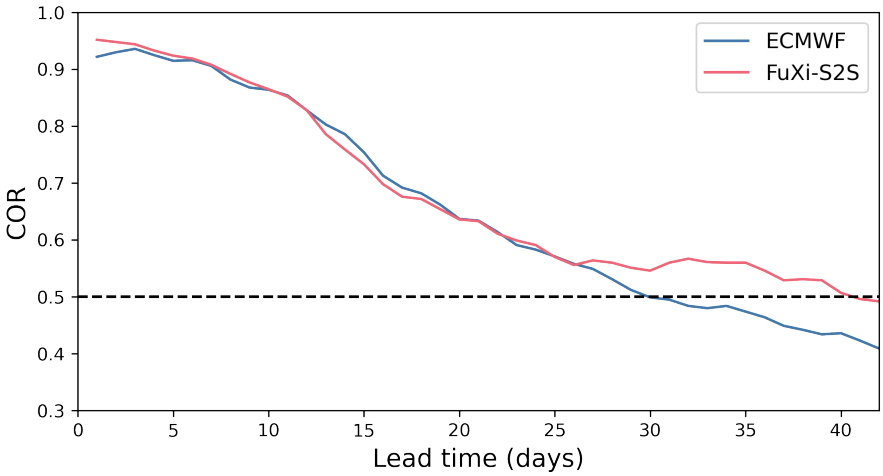


**Supplementary Figure 9**: Comparison of the globally-averaged latitude-weighted RMM bivariate COR (left column) of the ensemble mean of ECMWF S2S real-time forecasts (in blue) and FuXi-S2S forecasts (in red) using testing data from 2022, with dashed black lines indicating the prediction skill threshold of COR=0.5.

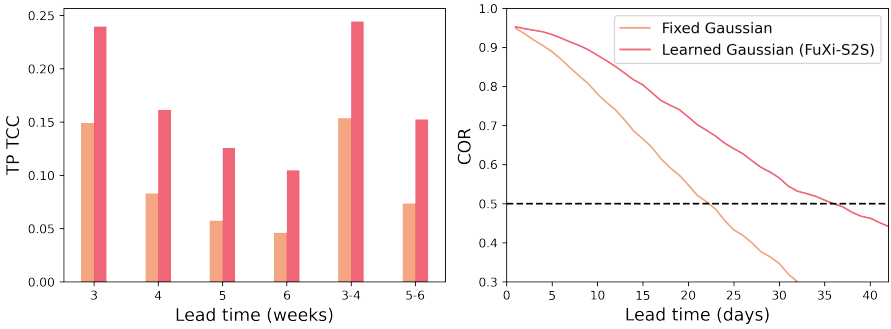


**Supplementary Figure 10**: Comparison of the FuXi-S2S model (in red) and FuXi-S2S with fixed Gaussian perturbations (in light red), utilizing all testing data from 2017 to 2021. The first column is the comparison of the globally-averaged latitude-weighted TCC. The second column is the comparison of the globally-averaged latitude-weighted RMM bivariate COR of the FuXi-S2S (in red) and FuXi-S2S with fixed Gaussian noise (in light red) using testing data from 2017 to 2021.

# References

[1] TAO, S.-Y.: A review of recent research on the east asian summer monsoon in china. Monsoon meteorology, 60–92 (1987)

[2] Ding, Y.: Summer monsoon rainfalls in china. Journal of the Meteorological Society of Japan. Ser. II **70**(1B), 373–396 (1992)

[3] Yihui, D., Chan, J.C.: The east asian summer monsoon: an overview. Meteorology and Atmospheric Physics **89**(1-4), 117–142 (2005)

[4] Liu, Y., Ding, Y.: Characteristics and possible causes for the extreme meiyu in 2020. Meteorological Monthly **46**(11), 1393–1404 (2020)

[5] Liu, B., Yan, Y., Zhu, C., Ma, S., Li, J.: Record-breaking meiyu rainfall around the yangtze river in 2020 regulated by the subseasonal phase transition of the north atlantic oscillation. Geophysical Research Letters **47**(22), 2020–090342 (2020)